

Softening of dd excitation in the resonant inelastic x-ray scattering spectra as a signature of Hund's coupling in nickelates

Umesh Kumar,¹ Corey Melnick,² and Gabriel Kotliar^{1,2}

¹*Department of Physics and Astronomy, Rutgers University, Piscataway, NJ 08854, USA*

²*Condensed Matter Physics and Materials Science Department,
Brookhaven National Laboratory, Upton, NY 11973, USA*

We investigate the effects of Hund's coupling on the resonant X-ray absorption spectra of the recently discovered family of layered nickelate superconductors. We contrast two scenarios depending on the relative strength of the ratio of the effective Hund's coupling (J_H) to the crystal fields (Δ) in these systems. We carry out the cluster and DFT+DMFT simulations of the RIXS signal at the Ni L -edge for different values of Hund's coupling. We find the latter dominates for the parent compound while the former becomes important for sufficiently large doping. Our results are consistent with the observations of a softening of a RIXS peak as a function of doping by Rossi *et al.* [1], only when the Hund coupling is sizeable. To interpret the results, we separate the theoretical RIXS signal into spin conserving and non-spin conserving channels and conclude that the infinite layer nickelates are in a regime where Δ and J compete effectively and suggest further experimental tests of the theory.

Introduction: A long-standing goal in condensed matter physics has been to discover a superconducting infinite-layer (IL) nickelate, as these compounds are analogous to the high-temperature two-dimensional (2D) superconducting cuprates [2], in which superconductivity was discovered in 1986 [3]. After a long search, superconductivity was discovered in the doped infinite layer nickelate, $\text{Nd}_{0.8}\text{Sr}_{0.2}\text{NiO}_2$ [4], with the differences in superconducting domes with the 2D cuprates [5, 6]. Recently, superconductivity was also reported in $\text{La}_3\text{Ni}_2\text{O}_7$, suggesting it as a generic feature of nickelates [7]. This is a major breakthrough, as the electronic structure of the nickelates is notably different from the cuprates. Most notably, the nickel in a nickelate is understood to exist in electron configurations from d^7 to d^9 , unlike the copper in a cuprate superconductor, which is understood to exist only in the d^9 configuration [8, 9]. Nickelates are also known to host metal-insulator transitions where the oxidation state of Ni plays a central role [9].

Superconductivity in doped 2D cuprates is understood to be driven by resonating valence bond states [10] and has d -wave pairing [11, 12]. This is usually explored using the Emery model [13], which allows for Zhang-Rice singlets formed with $d_{x^2-y^2}$ orbitals [14] and the oxygens. The parent compound for IL nickelate is weakly insulating in contrast to the Mott insulator realized in cuprates. The possibility of mixed oxidation states in nickelates makes the problem challenging, as multiple d orbitals can play a significant role in the origin of the superconductivity. In particular, $3z^2$ have been hypothesized to play a role in the ground state [15, 16]. The model for nickelates ranges from single-band to the multiorbitals of the Ni atom, and even the role of the rare-earth metal has been considered [16–27].

The Fermi surfaces of the rare earth metal have also been postulated to play a role in the IL nickelate NdNiO_2 [28–30], which complicates the understanding of the active degrees of freedom for superconductivity. The relevance of Hund's coupling has also been explored [30–

33]. More recently, it has been proposed that since these compounds are created by reduction, the hydrogen atoms in these materials can play a significant role, further complicating the description [34]. Indeed, the origin of superconductivity is a controversial topic, and the proposals are at a very nascent stage.

Recently, resonant inelastic x-ray scattering (RIXS) [1, 35–40] has also been extensively used to explore the relevant degrees of freedom in nickelates. It offers an advantage as it can amplify the response for smaller cross-sections, such as small crystals and thin films, due to large light-matter interaction and inherent resonance conditions in the technique. The spectroscopic response allows one to constrain the possible theory for superconductivity in nickelates. For example, In a recent study [39] on low valence nickelates, $\text{La}_4\text{Ni}_3\text{O}_8$ and $\text{La}_{2-x}\text{Sr}_x\text{CuO}_4$ revealed that the nickelates are of mixed charge-transfer–Mott–Hubbard character with the Coulomb repulsion U , in contrast to the charge-transfer nature of the cuprates in Zaanen–Sawatzky–Allen scheme. The distinction between dd excitations and charge transfer (CT) excitations helps to reveal the differences between the two. Recently, a softening of dd excitations in IL nickelate on doping was reported in Ni L -edge RIXS spectra [1]. We revisit the observation to investigate the relevance of Hund's coupling to the observation.

In this letter, we explore the dd excitations in undoped and doped nickelates. In the undoped case, dd excitation, the transition between singly occupied $d_{x^2-y^2}$ and other d orbitals is independent of J_H . In the doped case, there are two possible scenarios: i) $d_{x^2-y^2}$ is double occupied or ii) holes occupy $d_{x^2-y^2}$ and d_{3z^2} depending on the relative strength of the splitting between d orbitals (Δ) and J_H , which leads to either softening or hardening of dd excitations. Studying RIXS spectra using a small cluster and DFT+DMFT, we show that J_H plays a central role in softening dd excitations despite Δ dominating the ground state and report results consistent with the experimental softening of dd -excitations on doping [1].

Model:— We consider the Ni_2O_7 cluster shown in Fig. 1(a) with all the Ni 3d and O 2p orbitals, unless otherwise stated. The full Hamiltonian is given by $\mathcal{H} = \mathcal{H}_O + \mathcal{H}_C^d + \mathcal{H}_C^p + \mathcal{H}_{pd}$ [39]. The non-interacting part is

$$\begin{aligned} \mathcal{H}_0 = & \sum_{i\alpha} \epsilon_\alpha n_{i\alpha}^d + \sum_{i\mu} \epsilon_\mu n_{i\mu}^p + \sum_{\langle i\alpha, j\mu \rangle} t_{i\alpha, j\mu} d_{i\alpha\sigma}^\dagger p_{j\mu\sigma} \\ & + \sum_{\langle\langle i\mu, j\mu' \rangle\rangle, \sigma} t_{i\mu, j\mu'} p_{i\mu\sigma}^\dagger p_{j\mu'\sigma} + \text{h.c.} \end{aligned}$$

Here $\alpha \in \{d_{x^2-y^2}, d_{3z^2-r^2}, d_{xy}, d_{yz}, d_{zx}\}$ Ni 3d orbitals and $\mu \in \{p_x, p_y, p_z\}$ O 2p orbitals. $\epsilon_{\alpha/\mu}$ is the onsite energy at site i . $t_{i\alpha, j\beta}$ is hopping between orbital α of site i to β of j . $\mathcal{H}_{pd} = V_{pd} \sum_{ij} n_i^d n_j^p$. V_{dp} is nearest neighbor coulomb interaction. The Coulomb interaction on O atom is given by $H_C^p = U_p \sum_{i,\mu} n_{i\mu\uparrow}^p n_{i\mu\downarrow}^p$. \mathcal{H}_C^d is the Coulomb repulsion on the 3d of Ni are accounted for by the multiorbital Hubbard-Kanamori model [41–43] give by

$$\begin{aligned} \mathcal{H}_C^d = & U_d \sum_{i,\alpha} n_{i\alpha\uparrow}^d n_{i\alpha\downarrow}^d + U'_d \sum_{\substack{i,\sigma,\sigma', \\ \alpha < \beta}} n_{i\alpha\sigma} n_{i\beta\sigma'} \\ & + J_H \sum_{\substack{i,\sigma,\sigma', \\ \alpha < \beta}} d_{i\alpha\sigma}^\dagger d_{i\beta\sigma'}^\dagger d_{i\alpha\sigma'} d_{i\beta\sigma} + J_P \sum_{\substack{i,\sigma, \\ \alpha < \beta}} d_{i\alpha\sigma}^\dagger d_{i\alpha\sigma}^\dagger d_{i\beta\sigma} d_{i\beta\sigma} \end{aligned}$$

Here, U is the intraband Hubbard repulsion, U' , J_H , and J_P are interband Hubbard repulsion, Hund's exchange interaction, and pair hopping amplitude, respectively.

The parameters for this model for modeling nickelate and cuprates have been extensively reported in the literature and notably varied. In [supplement [44] Table I], we present the adapted non-interacting parameters from a few studies [15, 28, 45, 46]. The literature has a notably varied set of parameters, albeit all these studies agree that nickelates have large TM-ligand spitting and larger hopping overlap (t_{pd}) compared to cuprates. The relevant non-interacting parameters for this work are also shown in [supplement [44] Table I]. For the interacting part, we use $U_d = 6.5$, $U_p = 4.1$, $V_{pd} = 1.0$ and $J_H = 0.8$ (unless otherwise stated) for the nickelate model.

For evaluating the RIXS spectra, we consider the core-hole Hamiltonian given by $H_{\text{ch}} = \mathcal{H} + U_{\text{ch}} \sum_i n_i^d n_i^p$ for the L -edge [47, 48]. RIXS cross-section is evaluated using the Kramers-Heisenberg formula [35, 49, 50] given by,

$$\mathcal{I} = \sum_f \left| \sum_{i,n,\sigma} \frac{\langle f | \mathcal{D}^\dagger | n \rangle \langle n | \mathcal{D} | g \rangle}{E_n - E_g - \hbar\omega_{\text{in}} + i\Gamma_n} \right|^2 \delta(E_f - E_g - \Omega). \quad (1)$$

Here, $|g\rangle$, $|n\rangle$ and $|f\rangle$ are the ground, intermediate, and final states with energies E_g , E_n , and E_f respectively and $\Omega (= \hbar\omega_{\text{in}} - \hbar\omega_{\text{out}})$ is the energy loss of the incoming photon. Γ is the inverse core-hole lifetime. \mathcal{D} is dipole operator given by $\mathcal{D} = \sum_{i,\alpha,\sigma,J} e^{i\mathbf{k}\cdot\mathbf{R}_i} p_{i,\alpha,\sigma}^\dagger d_{i,\alpha,\sigma}$ for the Ni L -edge and involve core 2p (with spin-orbit coupling) and valence 3d shells of the nickel site. We evaluate spin-resolved Ni L -edge RIXS, where the angular dependence

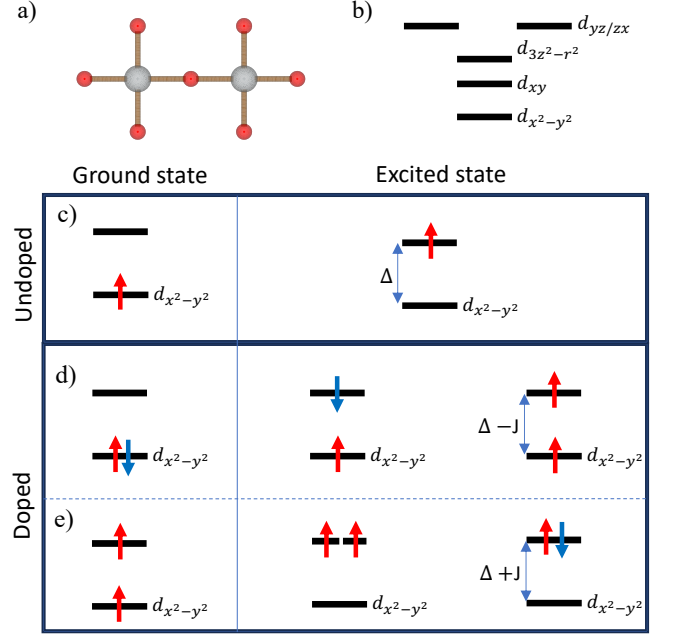


FIG. 1. Schematics of the cluster and the ground state occupancies in the cluster. a) shows the Ni_2O_7 cluster and b) shows its Ni 3d energy levels. c)-e) shows excitations for single ion configurations. c) shows schematics for the ground and dd transition for the undoped model. d) and e) show the schematics for ground and the dd transitions for the doped model with two ground state configurations; i) doubly occupied $d_{x^2-y^2}$ orbital for large Δ , and ii) one hole each in $d_{x^2-y^2}$ and $d_{3z^2-r^2}$ orbitals for large J_H , respectively. In the spin-flip ($\Delta S = 1$) channel, d) and e) will soften and harden dd excitations, respectively.

is integrated out, and the spectra are resolved into non-spin conserving (NSC, $\Delta S = 1$) and spin conserving (SC, $\Delta S = 0$) channels, depending on odd or even number of spin-flips in the excitations [37, 48, 51–53].

Results:— We now present results for the nickelates using a combination of techniques. The nickelate model allows for interesting scenarios, in particular for the doped case, as the doped nickelates model has larger occupancies on d -orbitals for the case of doped nickelates (also see supplement Fig. S2 [44]). We present nickelates RIXS spectra and investigate the origin of the softening in the RIXS spectra.

Fig. 1 shows the cluster considered in our work and schematics for the dd excitations. Panel (a) shows the Ni_2O_7 cluster considered later in our work, and panel (b) shows the energy Ni 3d onsite levels considered in our cluster. The Ni cluster with ligand can be mapped to energy levels for the single Ni site, integrating out the ligand (see supplement Sec. S2 for the mapping). We, therefore, start by considering the different scenarios of dd excitation for a single Ni ion (undoped: d^9 and doped: d^8) case. We consider that the lowest energy orbital is $d_{x^2-y^2}$, and other d orbitals are roughly separated by Δ energy gap in the hole language.

Panel c) presents the schematics for the dd excita-

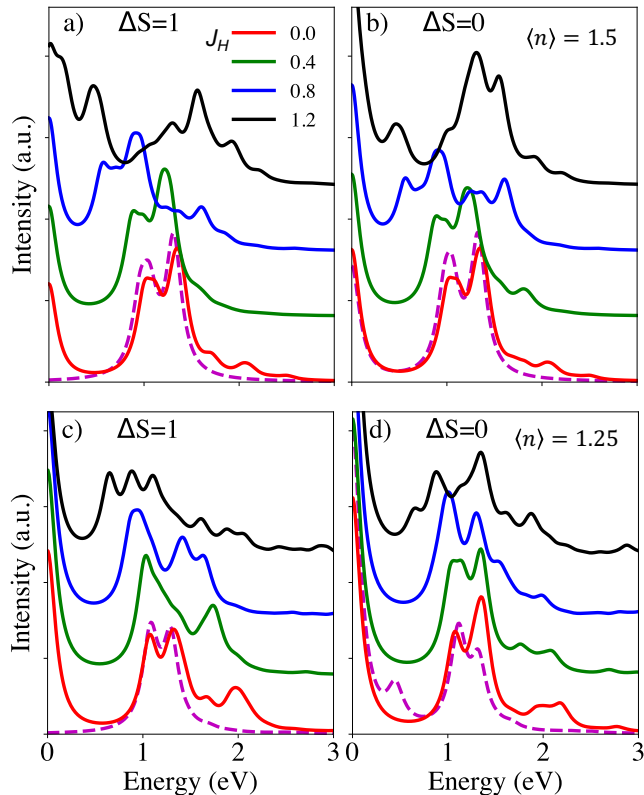


FIG. 2. Spin-resolved Ni L -edge RIXS spectra. a) and b) show results for Ni_2O_7 cluster in the NSC ($\Delta S = 1$) and SC ($\Delta S = 0$) channels. The dashed magenta line shows spectra for the undoped ($\langle n \rangle = 1$) model. Solid lines show spectra for the doped ($\langle n \rangle = 1.5$) model for the values of J_H mentioned in the legend. Similarly, c) and d) show results for Ni_4O_8 cluster in the NSC and SC channels, respectively, for undoped and doped ($\langle n \rangle = 1.25$) models.

tions realized in undoped single-site nickelates, where dd -excitations can be understood as simple excitations between $d_{x^2-y^2}$ to other d orbitals (Δ) as elucidated in the panel. In the doped case, there are two possible ground state configurations depending on the strength of J_H and Δ : i) $\Delta > J_H$: doubly occupied $d_{x^2-y^2}$, or ii) large $J_H > \Delta$: one hole each in $d_{x^2-y^2}$ and d_{z^2} (the preferential occupancy on this orbital is discussed later) as shown in panel d) and e) respectively. The NSC channel in d) leads to the softening of dd excitations. This configuration is also consistent with the ground state occupancy estimates. On the other hand, e) ground state will lead to hardening of the dd excitations. We use these schematic pictures as a guiding tool to understand the spectra in the models below.

RIXS spectra: We present the simulated RIXS spectra for a set of models to consider realistic doping to decipher the effect of J_H . We use Ni_2O_7 cluster to explore the undoped and hole-doped (50%) model. We additionally present results for a smaller doping (25%) model using Ni_4O_8 cluster and Anderson impurity model. To make Ni_4O_8 cluster computationally accessible, we neglect $d_{yz/zx}$ orbitals in the cluster [for details, see sup-

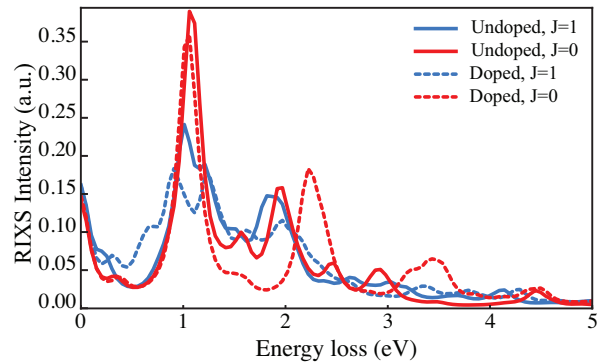


FIG. 3. RIXS spectra from the AIM for both the undoped and doped (0.25 hole doping) model. The results with and without J_H are shown in blue and red, respectively.

plement [44]]. Using these models, we examine the role of J_H in the spectra.

We start by examining the Ni L -edge RIXS spectra using Ni_2O_7 cluster with $(1 \uparrow, 1 \downarrow)$ and three $(2 \uparrow, 1 \downarrow)$ holes fillings to simulate the undoped and doped (50%) models in both the non spin-conserving (NSC, $\Delta S = 1$) and spin conserving (SC, $\Delta S = 0$) channels using KH formalism given by Eq. 1.

Panels a) and b) in Fig. 2 show NSC and SC channels of the Ni L -edge for the Ni_2O_7 cluster. The dashed magenta line shows the RIXS spectra for the undoped model and is independent of J_H . The doped (50%) model results are also shown in both panels using solid lines for a set of the J_H . The prominent peaks for the doped model $J_H = 0$ occur at the same energies as in the undoped case. We notice a softening of dd -excitation in both channels with the increase in J_H in both the NSC and SC channels. We will further revisit these results from this cluster later to examine the nature of the various peaks in both the channels.

To examine results for the lower doping (25%), we consider Ni_4O_8 cluster with $(3 \uparrow, 2 \downarrow)$ filling and evaluate the Ni L -edge RIXS spectra. Panels c) and d) case show results for both the undoped and doped models for this cluster. The dashed magenta line shows the RIXS spectra for the undoped model and is independent of J_H . In the SC channel, an additional bimagnon peak at around 0.3 eV [50, 54, 55] is observed for the undoped case. The large value of bimagnon can be attributed to the finite size of the cluster. The doped (25%) model results are shown using solid lines. The $J_H = 0$ case has the same characteristics as the undoped case. We observe softening of dd -excitation in both cases with an increase in J_H . We, therefore, observed softening here for realistic doping.

These cluster results reveal the softening of dd excitations on doping consistent with reported RIXS experiment on NdNiO_2 [1] and more recently in trilayer nickelates where the dd excitations were reported at even lower energies [40]. This shows that Hund's coupling is important for understanding the softening of dd excita-

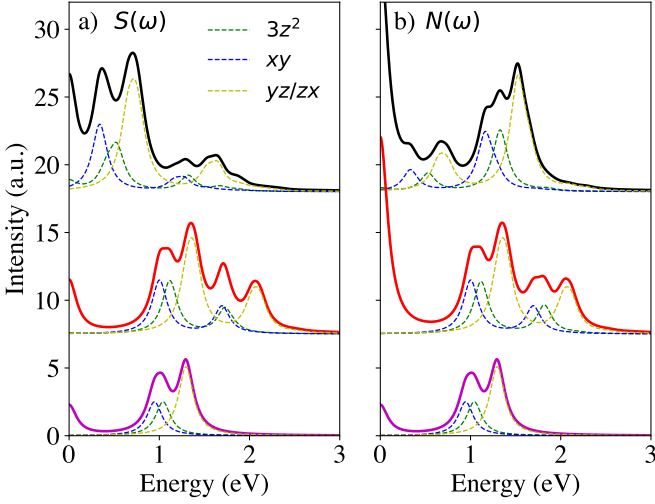


FIG. 4. $S(\omega)$ and $N(\omega)$ for the Ni_2O_7 cluster are shown in panel a) and b). Solid magenta shows the response for the undoped model. The dashed lines show the orbital-resolved excitations in the spectra. Solid red and black lines show response for the doped model with $J_H = 0$ and 1, respectively.

tions observed in nickelates.

We now present the RIXS spectra using an Anderson Impurity model (AIM) [see supplement S6 [44] and Ref. [36] for details] derived within charge self-consistent DFT+DMFT using Portobello [56–58]. The DFT+DMFT calculations are conducted with $U = 5$ eV and $J_H = 1$ and 0 eV using the GGA functional [59] and fully-localized limit double counting with a nominal Ni- d^8 valence. Fig. 3 shows the Ni L -edge RIXS spectra for the AIM. The undoped results are shown in solid lines using red and blue colors for $J_H = 0$ and $J_H = 1$, respectively. The dd -excitations exist at 1-2.5 eV and are minimally affected by J_H . The RIXS spectra for the doped model are shown in the dashed line in the respective colors. We find a significant softening of dd -excitations for the $J_H = 1$ case compared to the undoped case and the $J_H = 0$ of the doped case. This is consistent with our small cluster calculations and confirms the softening of dd -excitations observed in the experiment [1].

Dynamical spin and charge response:— The RIXS response given by Eq. 1 is complex; we, therefore, examine the model in the $\Gamma_n \rightarrow \infty$ limit, in which the core-hole effects are eliminated. We evaluate the dynamical spin ($S(\omega)$, $\Delta S = 1$) and charge ($N(\omega)$, $\Delta S = 0$) response on the Ni_2O_7 cluster. Fig. 4 shows the $S(\omega)$ and $N(\omega)$ response in the panel a) and b), respectively. The undoped model results are shown in magenta solid line for $J_H = 1.2$ and the doped model in red and black lines for $J_H = 0$ and 1, respectively. We also plot the orbital resolved spectra where the outgoing dipole operator in Eq. 1 is restricted to a single orbital, which allows us to identify the different dd -excitations. In both spectra, the ordering of the orbital excitations with energy less is as follows for the undoped model: d_{xy} , d_{3z^2} ,

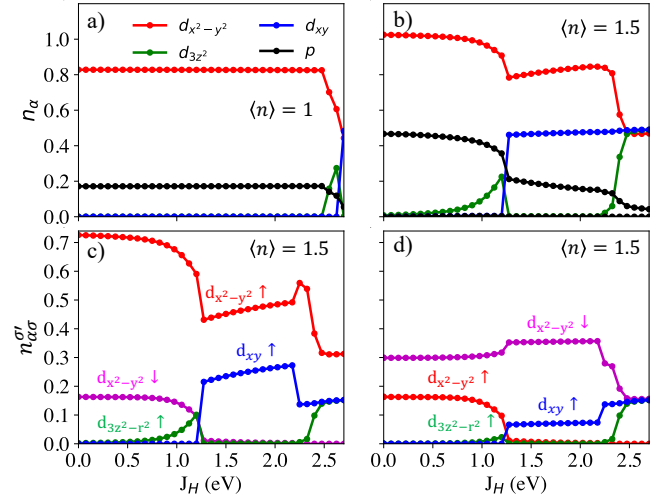


FIG. 5. Ground state analysis of the Ni_2O_7 cluster. a) and b) show the orbital resolved n_α dependence on J_H for undoped ($\langle n \rangle = 1$) and doped ($\langle n \rangle = 1.5$), respectively. c) and d) show the spin-resolved orbital double occupancies ($n_{\alpha\sigma}[n_{d_{x^2-y^2}\sigma'}]$) on the Ni site in the doped case for $\sigma' = \uparrow$ and \downarrow , respectively.

and then $d_{yz/zx}$. This hierarchy of dd excitations differs from Ref. [1] which reports that $3z^2$ is the highest excitations in NdNiO_2 using the polarization dependence of the excitations. We re-examine the data in [see supplement S5 [44]] and show that assigning d_{3z^2} the lower energy excitations compared to $d_{yz/zx}$ orbital excitation can also reproduce the observed polarization dependence, as these orbitals have similar angular dependence within the reported experimental resolutions.

In the doped model, the results are sensitive to J_H . For $J_H = 0$, the orbital resolved dd -excitations has primarily two peaks, with the bright lower energy peaks coinciding with the undoped case. For $J_H = 1$, we find that the prominent excitations soften in the $S(\omega)$ channel, consistent with the RIXS results. This contrasts with the $N(\omega)$, where mild hardening is observed, and the softening in SC channel of RIXS can be described as a consequence of finite core-hole lifetime.

Fig. 5 shows the results for the analysis of the ground state dependence on J_H in the undoped ($\langle n \rangle = 1$) and doped ($\langle n \rangle = 1.5$). Panel a) shows results for the undoped model. Here, the occupancies in the Ni $3d$ orbitals (n_α) in the ground state, which is given by $n_\alpha = \langle g | \sum_\sigma n_{i,\alpha,\sigma} | g \rangle$ dependence on J_H are presented. We find that the holes are restricted to $d_{x^2-y^2}$ orbital and the oxygen p orbitals. Other d -orbitals do not contribute to the ground state for reasonable J_H .

Panels b)-d) shows the ground state results for the doped model. Panel b) shows n_α dependence on J_H . For small J_H , the has holes restricted to the $d_{x^2-y^2}$ orbital and O $2p$ orbitals, the occupancy on d_{3z^2} increases with J_H till 1.25 eV, where it reaches around 20% of $d_{x^2-y^2}$. This is despite d_{xy} having a lower onsite energy. The dominant weight on d_{3z^2} can be attributed to the large hopping and the oxygen p -orbitals shared between the two d -orbitals (also see Fig. S1 in supplement [44]).

For $J_H = 1.25 - 2.25$ eV, the d_{xy} orbital becomes occupied with 60% the occupancy of the $d_{x^2-y^2}$ orbital. For the unphysical $J_H > 2.5$ eV, these three orbitals are almost equally occupied. To investigate where the extra hole resides, we plot the constrained occupancies, $n_{\alpha\sigma}^{\sigma'} = \langle g | n_{d_{\alpha\sigma}} [n_{d_{x^2-y^2\sigma'}}] | g \rangle$. The occupancy on $d_{x^2-y^2}$ with spin $\sigma' = \uparrow$ and \downarrow is constrained and are shown in panels c) and d), respectively. For small J_H , the $d_{x^2-y^2}$ has double occupancy, which is expected due to the penalty of the CF-splitting. We notice an increase in occupancy on d_{3z^2} with $\sigma = \sigma'$ mediated by Hund's coupling till $J_H = 1.25$ eV. This makes the scenario discussed in Fig. 1(d) relevant for the nickelates, which leads to the softening of dd excitations.

Conclusions:— In this work, we have explored the effects of Hund's coupling in undoped and doped nickelates using small cluster models and DMFT. Using these models, we find that Hund's coupling plays a central role in softening the dd excitations and softening is enhanced

for larger doping. This softening of dd -excitations with the increase in doping is consistent with the recent report experimental study of IL nickelates [1]. Our small cluster analysis shows that doubly occupied $d_{x^2-y^2}$ is the preferred state for the doped nickelates, but the dd excitations are softened due to lowering of the dd excitations in the RIXS spectra. This contrasts with the cuprate, where the extra hole typically resides on the ligands [14].

Future experiments using photon polarization dependent RIXS that allow for spin resolution [60]. They will test the relative contributions of spin and charge fluctuations to the RIXS signal. Comparison with simulations will further help one clarify the minimal model for the nickelates. Also, a comparative study of dd excitations nickelates and cuprates can be a useful tool to highlight the difference between the two.

This work was supported by the US Department of Energy, Office of Basic Energy Sciences, as part of the Computation Material Science Program.

-
- [1] M. Rossi, H. Lu, A. Nag, D. Li, M. Osada, K. Lee, B. Y. Wang, S. Agrestini, M. Garcia-Fernandez, J. J. Kas, Y.-D. Chuang, Z. X. Shen, H. Y. Hwang, B. Moritz, K.-J. Zhou, T. P. Devereaux, and W. S. Lee, *Phys. Rev. B* **104**, L220505 (2021).
- [2] V. I. Anisimov, D. Bukhalov, and T. M. Rice, *Phys. Rev. B* **59**, 7901 (1999).
- [3] J. G. Bednorz and K. A. Müller, *Zeitschrift für Physik B Condensed Matter* **64**, 189 (1986).
- [4] D. Li, K. Lee, B. Y. Wang, M. Osada, S. Crossley, H. R. Lee, Y. Cui, Y. Hikita, and H. Y. Hwang, *Nature* **572**, 624 (2019).
- [5] D. Li, B. Y. Wang, K. Lee, S. P. Harvey, M. Osada, B. H. Goodge, L. F. Kourkoutis, and H. Y. Hwang, *Phys. Rev. Lett.* **125**, 027001 (2020).
- [6] L. Taillefer, *Annual Review of Condensed Matter Physics* **1**, 51 (2010).
- [7] H. Sun, M. Huo, X. Hu, J. Li, Z. Liu, Y. Han, L. Tang, Z. Mao, P. Yang, B. Wang, J. Cheng, D.-X. Yao, G.-M. Zhang, and M. Wang, *Nature* (2023), 10.1038/s41586-023-06408-7.
- [8] M. Hepting, M. P. M. Dean, and W.-S. Lee, *Frontiers in Physics* **9** (2021), 10.3389/fphy.2021.808683.
- [9] S. Johnston, A. Mukherjee, I. Elfimov, M. Berciu, and G. A. Sawatzky, *Phys. Rev. Lett.* **112**, 106404 (2014).
- [10] P. W. Anderson, *Science* **235**, 1196 (1987).
- [11] G. Kotliar, *Phys. Rev. B* **37**, 3664 (1988).
- [12] G. Kotliar and J. Liu, *Phys. Rev. B* **38**, 5142 (1988).
- [13] V. J. Emery, *Phys. Rev. Lett.* **58**, 2794 (1987).
- [14] F. C. Zhang and T. M. Rice, *Phys. Rev. B* **37**, 3759 (1988).
- [15] C.-J. Kang and G. Kotliar, *Phys. Rev. Lett.* **126**, 127401 (2021).
- [16] F. Lechermann, *Phys. Rev. X* **10**, 041002 (2020).
- [17] L.-H. Hu and C. Wu, *Phys. Rev. Res.* **1**, 032046 (2019).
- [18] P. Werner and S. Hoshino, *Phys. Rev. B* **101**, 041104 (2020).
- [19] M. Hirayama, T. Tadano, Y. Nomura, and R. Arita, *Phys. Rev. B* **101**, 075107 (2020).
- [20] Y.-H. Zhang and A. Vishwanath, *Phys. Rev. Res.* **2**, 023112 (2020).
- [21] Z. Wang, G.-M. Zhang, Y.-f. Yang, and F.-C. Zhang, *Phys. Rev. B* **102**, 220501 (2020).
- [22] F. Petocchi, V. Christiansson, F. Nilsson, F. Aryasetiawan, and P. Werner, *Phys. Rev. X* **10**, 041047 (2020).
- [23] X. Wu, D. Di Sante, T. Schwemmer, W. Hanke, H. Y. Hwang, S. Raghu, and R. Thomale, *Phys. Rev. B* **101**, 060504 (2020).
- [24] Y. Gu, S. Zhu, X. Wang, J. Hu, and H. Chen, *Communications Physics* **3**, 84 (2020).
- [25] E. Been, W.-S. Lee, H. Y. Hwang, Y. Cui, J. Zaanen, T. Devereaux, B. Moritz, and C. Jia, *Phys. Rev. X* **11**, 011050 (2021).
- [26] M. Jiang, M. Berciu, and G. A. Sawatzky, *Phys. Rev. Lett.* **124**, 207004 (2020).
- [27] M. Kitatani, L. Si, O. Janson, R. Arita, Z. Zhong, and K. Held, *npj Quantum Materials* **5**, 59 (2020).
- [28] M. Hepting, D. Li, C. J. Jia, H. Lu, E. Paris, Y. Tseng, X. Feng, M. Osada, E. Been, Y. Hikita, Y.-D. Chuang, Z. Hussain, K. J. Zhou, A. Nag, M. Garcia-Fernandez, M. Rossi, H. Y. Huang, D. J. Huang, Z. X. Shen, T. Schmitt, H. Y. Hwang, B. Moritz, J. Zaanen, T. P. Devereaux, and W. S. Lee, *Nature Materials* **19**, 381 (2020).
- [29] K. Higashi, M. Winder, J. Kuneš, and A. Hariki, *Phys. Rev. X* **11**, 041009 (2021).
- [30] Y. Wang, C.-J. Kang, H. Miao, and G. Kotliar, *Phys. Rev. B* **102**, 161118 (2020).
- [31] H.-S. Jin, W. E. Pickett, and K.-W. Lee, *Journal of Physics: Materials* **5**, 024008 (2022).
- [32] J. Chang, J. Zhao, and Y. Ding, *The European Physical Journal B* **93**, 220 (2020).
- [33] B. Kang, C. Melnick, P. Semon, S. Rye, M. J. Han, G. Kotliar, and S. Choi, *npj Quantum Materials* **8**, 35 (2023).
- [34] X. Ding, C. C. Tam, X. Sui, Y. Zhao, M. Xu, J. Choi, H. Leng, J. Zhang, M. Wu, H. Xiao, X. Zu, M. Garcia-Fernandez, S. Agrestini, X. Wu, Q. Wang, P. Gao, S. Li,

- B. Huang, K.-J. Zhou, and L. Qiao, *Nature* **615**, 50 (2023).
- [35] L. J. P. Ament, M. van Veenendaal, T. P. Devereaux, J. P. Hill, and J. van den Brink, *Rev. Mod. Phys.* **83**, 705 (2011).
- [36] Y. Wang, G. Fabbris, M. Dean, and G. Kotliar, *Computer Physics Communications* **243**, 151 (2019).
- [37] U. Kumar, A. Nag, J. Li, H. C. Robarts, A. C. Walters, M. García-Fernández, R. Saint-Martin, A. Revcolevschi, J. Schlappa, T. Schmitt, S. Johnston, and K.-J. Zhou, *Phys. Rev. B* **106**, L060406 (2022).
- [38] M. Rossi, M. Osada, J. Choi, S. Agrestini, D. Jost, Y. Lee, H. Lu, B. Y. Wang, K. Lee, A. Nag, Y.-D. Chuang, C.-T. Kuo, S.-J. Lee, B. Moritz, T. P. Devereaux, Z.-X. Shen, J.-S. Lee, K.-J. Zhou, H. Y. Hwang, and W.-S. Lee, *Nature Physics* **18**, 869 (2022).
- [39] Y. Shen, J. Sears, G. Fabbris, J. Li, J. Pellicciari, I. Jarrige, X. He, I. Božović, M. Mitran, J. Zhang, J. F. Mitchell, A. S. Botana, V. Bisogni, M. R. Norman, S. Johnston, and M. P. M. Dean, *Phys. Rev. X* **12**, 011055 (2022).
- [40] Y. Shen, J. Sears, G. Fabbris, J. Li, J. Pellicciari, M. Mitran, W. He, J. Zhang, J. F. Mitchell, V. Bisogni, M. R. Norman, S. Johnston, and M. P. M. Dean, *Phys. Rev. X* **13**, 011021 (2023).
- [41] E. Dagotto, T. Hotta, and A. Moreo, *Physics Reports* **344**, 1 (2001).
- [42] A. M. Oleś, G. Khaliullin, P. Horsch, and L. F. Feiner, *Phys. Rev. B* **72**, 214431 (2005).
- [43] U. Kumar, S. Banerjee, and S.-Z. Lin, *Communications Physics* **5**, 157 (2022).
- [44] See Supplemental Material at, Link to be added by publisher, parameter tables, Angular dependence and etc., and includes Refs. [52].
- [45] A. S. Botana and M. R. Norman, *Phys. Rev. X* **10**, 011024 (2020).
- [46] J. Karp, A. S. Botana, M. R. Norman, H. Park, M. Zingl, and A. Millis, *Phys. Rev. X* **10**, 021061 (2020).
- [47] A. Nocera, U. Kumar, N. Kaushal, G. Alvarez, E. Dagotto, and S. Johnston, *Scientific Reports* **8**, 11080 (2018).
- [48] U. Kumar, A. Nocera, E. Dagotto, and S. Johnston, *Phys. Rev. B* **99**, 205130 (2019).
- [49] U. Kumar, A. Nocera, E. Dagotto, and S. Johnston, *New Journal of Physics* **20**, 073019 (2018).
- [50] J. Schlappa, U. Kumar, K. J. Zhou, S. Singh, M. Mourigal, V. N. Strocov, A. Revcolevschi, L. Patthey, H. M. Rønnow, S. Johnston, and T. Schmitt, *Nature Communications* **9**, 5394 (2018).
- [51] S. Kourtis, J. van den Brink, and M. Daghofer, *Phys. Rev. B* **85**, 064423 (2012).
- [52] C. Jia, K. Wohlfeld, Y. Wang, B. Moritz, and T. P. Devereaux, *Phys. Rev. X* **6**, 021020 (2016).
- [53] M. Moretti Sala, V. Bisogni, C. Aruta, G. Balestrino, H. Berger, N. B. Brookes, G. M. d. Luca, D. Di Castro, M. Grioni, M. Guarise, P. G. Medaglia, F. Miletto Granozio, M. Minola, P. Perna, M. Radovic, M. Salluzzo, T. Schmitt, K. J. Zhou, L. Braicovich, and G. Ghiringhelli, *New Journal of Physics* **13**, 043026 (2011).
- [54] V. Bisogni, L. Simonelli, L. J. P. Ament, F. Forte, M. Moretti Sala, M. Minola, S. Huotari, J. van den Brink, G. Ghiringhelli, N. B. Brookes, and L. Braicovich, *Phys. Rev. B* **85**, 214527 (2012).
- [55] S. Pal, U. Kumar, Prabhakar, and A. Mukherjee, (2023), [arXiv:2305.00802](https://arxiv.org/abs/2305.00802).
- [56] A. Kutepov, K. Haule, S. Y. Savrasov, and G. Kotliar, *Phys. Rev. B* **85**, 155129 (2012).
- [57] C. Melnick, P. Sémon, K. Yu, N. D’Imperio, A.-M. Tremblay, and G. Kotliar, *Computer Physics Communications* **267**, 108075 (2021).
- [58] *Computer. Phys. Commun.* **294**, 108907 (2023).
- [59] J. P. Perdew, K. Burke, and M. Ernzerhof, *Physical Review Letters* **77**, 3865 (1996), publisher: American Physical Society.
- [60] L. Martinelli, D. Betto, K. Kummer, R. Arpaia, L. Braicovich, D. Di Castro, N. B. Brookes, M. Moretti Sala, and G. Ghiringhelli, *Phys. Rev. X* **12**, 021041 (2022).
- [61] J. Q. Lin, P. Villar Arribi, G. Fabbris, A. S. Botana, D. Meyers, H. Miao, Y. Shen, D. G. Mazzone, J. Feng, S. G. Chiuzbaian, A. Nag, A. C. Walters, M. García-Fernández, K.-J. Zhou, J. Pellicciari, I. Jarrige, J. W. Freeland, J. Zhang, J. F. Mitchell, V. Bisogni, X. Liu, M. R. Norman, and M. P. M. Dean, *Phys. Rev. Lett.* **126**, 087001 (2021).
- [62] H. Lu, M. Rossi, A. Nag, M. Osada, D. F. Li, K. Lee, B. Y. Wang, M. Garcia-Fernandez, S. Agrestini, Z. X. Shen, E. M. Been, B. Moritz, T. P. Devereaux, J. Zaanen, H. Y. Hwang, K.-J. Zhou, and W. S. Lee, *Science* **373**, 213 (2021).
- [63] Q. Gao, S. Fan, Q. Wang, J. Li, X. Ren, I. Bialo, A. Drewanowski, P. Rothenbühler, J. Choi, Y. Wang, T. Xiang, J. Hu, K.-J. Zhou, V. Bisogni, R. Comin, J. Chang, J. Pellicciari, X. J. Zhou, and Z. Zhu, “Magnetic excitations in strained infinite-layer nickelate pnio2,” (2022), [arXiv:2208.05614](https://arxiv.org/abs/2208.05614).
- [64] U. Kumar and S.-Z. Lin, *Phys. Rev. B* **103**, 064508 (2021).
- [65] B. H. Goodge, D. Li, K. Lee, M. Osada, B. Y. Wang, G. A. Sawatzky, H. Y. Hwang, and L. F. Kourkoutis, *Proceedings of the National Academy of Sciences* **118**, e2007683118 (2021).
- [66] B. H. Goodge, B. Geisler, K. Lee, M. Osada, B. Y. Wang, D. Li, H. Y. Hwang, R. Pentcheva, and L. F. Kourkoutis, *Nature Materials* **22**, 466 (2023).
- [67] K. Ishii, T. Tohyama, S. Asano, K. Sato, M. Fujita, S. Wakimoto, K. Tustsui, S. Sota, J. Miyawaki, H. Niwa, Y. Harada, J. Pellicciari, Y. Huang, T. Schmitt, Y. Yamamoto, and J. Mizuki, *Phys. Rev. B* **96**, 115148 (2017).
- [68] Y. Matsubayashi and S. Ishihara, *Phys. Rev. B* **107**, 075121 (2023).

Supplement for “Softening of dd excitation in the resonant inelastic x-ray scattering spectra as a signature of Hund’s coupling in nickelates”

S1. PARAMETERS FOR THE MODEL HAMILTONIAN

A number of studies have reported relevant parameters for the nickelates and cuprates. In Table I, we present the adapted parameters from a few studies. The literature has a notably varied set of parameters. Still, all these studies report smaller $3d$ -orbitals crystal field splitting compared to the cuprates. Additionally, larger hopping overlap (t_{pd}) and oxygen p onsite energies (Δ_{pd}) are reported for nickelates.

		ϵ_{3z^2}	ϵ_{xy}	$\epsilon_{yz/zx}$	Δ_{pd}	t_{pd}
Ref. [45]	LaNiO ₂	0.71	0.73	0.63	4.4	1.23
	CaCuO ₂	0.97	1.04	0.93	2.69	1.20
Ref. [46]	NdNiO ₂	0.14	-	-	3.3	1.37
	CaCuO ₂	0.56	-	-	2.1	1.27
Ref. [39]	La ₄ Ni ₃ O ₈	0.2	0.1	0.3	5.6	1.36
	La _{2-x} Sr _x CuO ₄	0.95	0.7	0.9	4.0	1.17
Ref. [28]	LaNiO ₂	0.74	0.8	0.70	3.96	1.20
Ref. [15]	LaNiO ₂	0.38	2.03	1.40	-	-
This work	Ni cluster	0.2	0.1	0.3	5.6	1.36
	Cu cluster	0.95	0.7	0.9	4.0	1.17

TABLE I. Parameters reported in the literature for nickelates and their comparison with cuprates. The onsite energies are with respect to the $\epsilon_{x^2-y^2}$ as a reference in the hole language. Δ_{pd} is the onsite energy of oxygen p -orbitals with respect to the $\epsilon_{x^2-y^2}$. t_{pd} is the overlap of $d_{x^2-y^2}$ and oxygen p orbitals.

In this work, we use the parameters shown in Table I, motivated by Ref. [39]. We use the relation; $V_{pd\pi} = -V_{pd\sigma}/2$ and $V_{pp\pi} = -V_{pp\sigma}/4$ to evaluate the hopping parameters between other orbitals shown in Fig. S1. We also use; $U_d = 6.5$, $U_p = 4.1$ and $J_H = 0.8$ (unless otherwise stated) for the nickelates. These parameters are consistent with the observed superexchange in TL nickelates [61] (*i.e.* 69 meV) and IL nickelates (*i.e.* 64 meV) [62, 63]. As $J \approx 4 \frac{t_{pd}^4}{\Delta_{pd}^2 U_d}$, the large value of t_{pd} allows for a significant superexchange in spite of the large Δ_{pd} [26, 64].

S2. MAPPING TMO₄ CLUSTER TO ONE-SITE CLUSTER

In the TMO₄ plaquettes at half-filling (one hole in the cluster), hybridized energies of states for $d_{x^2-y^2}$ orbitals (see Fig. S1(a)) can be estimated using

$$H = \mathbf{C}^\dagger \begin{pmatrix} 0 & -t_{pd} & t_{pd} & t_{pd} & -t_{pd} \\ -t_{pd} & \Delta_{pd} & t_{pp} & 0 & -t_{pp} \\ t_{pd} & t_{pp} & \Delta_{pd} & -t_{pp} & 0 \\ t_{pd} & 0 & -t_{pp} & \Delta_{pd} & t_{pp} \\ -t_{pd} & -t_{pp} & 0 & t_{pp} & \Delta_{pd} \end{pmatrix} \mathbf{C} \quad (\text{S1})$$

Here, $\mathbf{C}^\dagger = (d_\alpha^\dagger \ p_{\alpha,+x}^\dagger \ p_{\alpha,+y}^\dagger \ p_{\alpha,-x}^\dagger \ p_{\alpha,-y}^\dagger)$. Similarly, one can write the Hamiltonian associated with other d -orbitals. The lowest eigen-energies for the d -orbitals are given by

$$\begin{aligned} E_{x^2-y^2} &= \frac{1}{2} \left(\tilde{\Delta}_- - \sqrt{16t_{pd}^2 + \tilde{\Delta}_-^2} \right) \\ E_{3z^2/xy} &= \frac{1}{2} \left(\tilde{\Delta}_+ + \epsilon_\alpha - \sqrt{16T_\alpha^2 + (\tilde{\Delta}_+ - \epsilon_\alpha)^2} \right) \\ E_{yz/zx} &= \frac{1}{2} \left(\Delta + \epsilon_\alpha - \sqrt{8T_\alpha^2 + (\Delta - \epsilon_\alpha)^2} \right) \end{aligned} \quad (\text{S2})$$

Here $\tilde{\Delta}_\pm = \Delta_{pd} \pm 2t_{pp}$ and ϵ_α and T_α are the respective on-site energy and hopping integral for the respective d -orbitals. Notice that the oxygen onsite energies are renormalized differently for $x^2 - y^2$ orbitals and the $3z^2/xy$

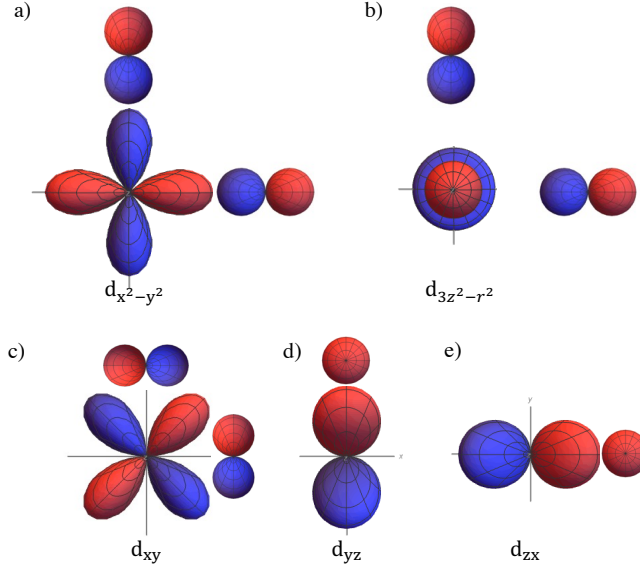


FIG. S1. Top view of the hopping overlaps for the d orbitals with the adjacent oxygen orbitals. a) and b) show $d_{x^2-y^2}$ and $d_{3z^2-r^2}$ overlap with the same oxygen p -orbitals, in contrast to other d -orbitals shown in c)-e), which hybridize with the other oxygen p -orbitals.

orbitals due to distinct phases in these orbitals. The Δ_{pd} for yz/zx is unaffected as we consider hopping only in the xy -plane, see Fig. S1(d)-(e). Using the parameters in Table I, the dd-excitations therefore associated with various excitations, in the limit, $\{t_{pd}, t_{pp}, \epsilon\} \ll \Delta_{pd}$, can be approximate to

$$\begin{aligned}
 \Delta E_{3z^2} &\approx \epsilon_{3z^2} + \frac{4t_{pd}^2}{3\Delta_{pd}} \left(2 + \frac{8t_{pp}}{\Delta_{pd}} - \frac{\epsilon_{3z^2}}{\Delta_{pd}} \right) \\
 \Delta E_{xy} &\approx \epsilon_{xy} + \frac{4t_{pd}^2}{4\Delta_{pd}} \left(3 + \frac{10t_{pp}}{\Delta_{pd}} - \frac{\epsilon_{xy}}{\Delta_{pd}} \right) \\
 \Delta E_{yz/zx} &\approx \epsilon_{yz/zx} + \frac{4t_{pd}^2}{8\Delta_{pd}} \left(7 + \frac{16t_{pp}}{\Delta_{pd}} - \frac{\epsilon_{yz/zx}}{\Delta_{pd}} \right)
 \end{aligned} \tag{S3}$$

These energy differences give an estimate for the dd excitations for the undoped model. Notice that the hybridized dd -excitation depends on the onsite energies. Also, the t_{pd}^2/Δ_{pd} is significant and can, therefore, strongly renormalize the dd -excitations.

S3. GROUND STATE ANALYSIS

To understand our model in a simplistic case with all the interactions, we explore the TMO_4 cluster with $3d$ of TM (transition metal) and $2p$ oxygen orbitals in the model. We highlight the differences between the model for nickelate and cuprates. The d^9 and d^8 configurations suggest that the multiorbital effects are important for nickelates compared to the models used for cuprates.

TMO₄ cluster:— Fig S2 shows the ground state orbital resolved occupancy results for one and two holes in NiO_4 cluster and CuO_4 clusters. Panel a) shows orbital-resolved occupancy results for NiO_4 cluster dependence on the onsite energy of ϵ_{3z^2} for NiO_4 cluster for one and two holes, respectively. Similarly, panel b) shows the results for the CuO_4 cluster. We notice that the ground state for the one hole is restricted to the $d_{x^2-y^2}$ orbital in both the case and hybridized with the ligands. This is because the Coulomb terms cannot act on a single hole. In the case of two holes, the NiO_4 plotted for $J_H = 1.2$ has the additional hole residing on the $d_{3z^2-r^2}$ till $\epsilon_{3z^2} \approx \epsilon_{xy}$ after that the hole instead resides on d_{xy} . In contrast, the extra hole resides on the ligand in CuO_4 model due to smaller onsite ligand energies. The milder dependence increase in oxygen site occupancy in nickelates is supported by the electron energy loss spectroscopy (EELS) on oxygen K -edge of nickelates [65, 66] with doping in contrast to the large increase in oxygen occupancy of hole-doped cuprates [67].

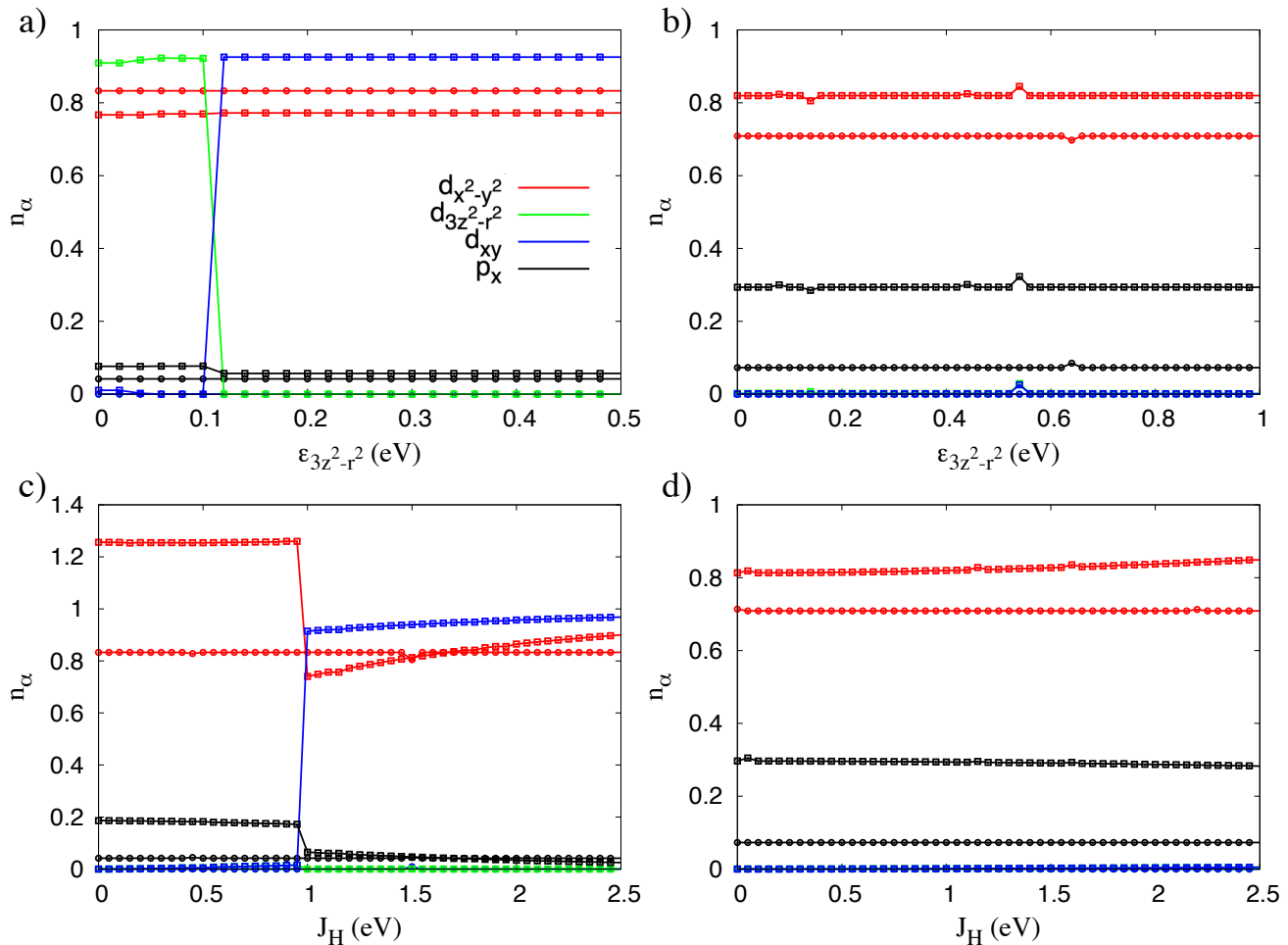


FIG. S2. Orbitals occupancy for the one (*i.e.* d^9) and two (*i.e.* d^8) holes in the TMO_4 clusters. a) and c) show the orbital-resolved occupancy results for NiO_4 cluster dependence on tetragonal distortion, characterized by ϵ_{3z^2} and J_H , respectively. b) and d) show the orbital-resolved occupancy results for the CuO_4 cluster. Open circles (\circ) and squares (\square) plot the results for one and two holes, respectively.

Panel c) and d) show the orbital-resolved occupancy results for NiO_4 and CuO_4 clusters, respectively, dependence on J_H . Again in the single hole case, the hole is restricted to $d_{x^2-y^2}$ -orbital and hybridized with ligands for both clusters. In the case of two holes, we notice that for small $J_H < 1$ in NiO_4 cluster, the extra hole resides on the $d_{x^2-y^2}$. Beyond this, the extra hole resides on the d_{xy} orbital and the relevant oxygen orbitals. Instead for the CuO_4 cluster, the extra hole always resides on the ligand side, consistent with the charge-transfer picture of cuprates.

While the single site model can only account for the local effects, our model shows that the single d orbital picture works for both the nickelate and cuprate in the undoped model. In the doped model, multiple orbitals can play a significant role for nickelate, in contrast to cuprates where occupancy is still restricted to $d_{x^2-y^2}$ along with the extra hole preferentially residing on the ligand.

We have reported the results for the Ni_2O_7 cluster in the main text. We present results for Ni_4O_8 cluster without $d_{yz/zx}$ orbitals in the cluster to make it computationally accessible.

Ni_4O_8 cluster:— Here, we report the results for the state-of-the-art Ni_4O_8 cluster, which allows for 25% doping ($d^{8.75}$) in the model Hamiltonian cluster. To make this computationally accessible, we integrate out the $d_{yz/zx}$ -orbitals as these do not contribute to the ground state, as is evident from the smaller cluster work. The reduced Hilbert space, therefore, allows us to explore 1.25 hole/site (*i.e.* $d^{8.75}$) in the cluster, which is relatively close to the superconducting IL-nickelates [5]. We use periodic boundary conditions for this model.

Fig. S3 shows the n_α dependence on J_H in the ground state for this cluster. Panel a) shows results for the undoped

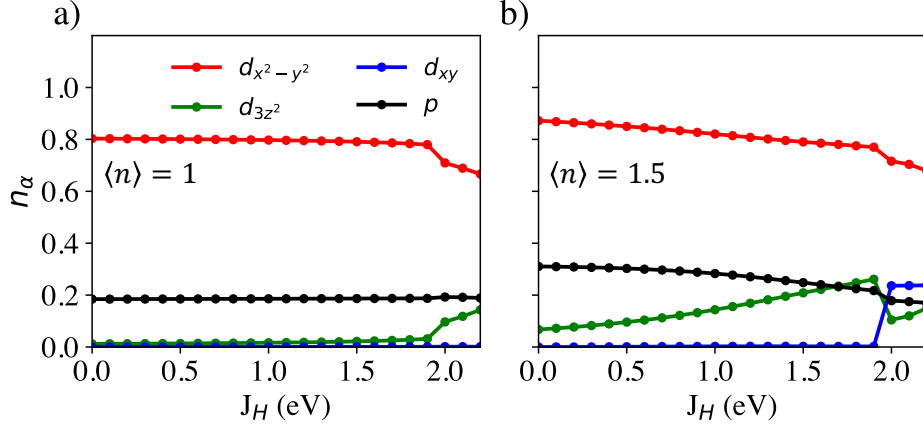


FIG. S3. Orbital resolved occupancies in the ground state of Ni_4O_8 cluster. a) shows the dependence of orbital-resolved occupancies on J_H for the undoped cluster, and b) shows the dependence of orbital-resolved occupancies on J_H for the doped (25%) cluster.

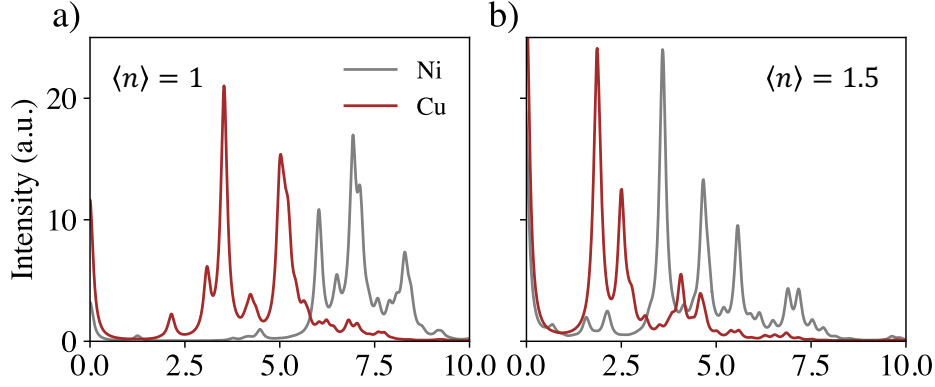


FIG. S4. Oxygen K -edge RIXS spectra for $\text{TM}(=\text{Ni}, \text{Cu})_2\text{O}_7$ cluster. a) and b) show the spectra for the undoped and doped models, respectively. The gray (brown) line in each panel shows the spectra for nickelate (cuprates) models.

model. The ground state occupancies are unaffected by Hund's coupling for reasonable values of J_H (< 1.8), consistent with the other clusters. The holes are hybridized between $d_{x^2-y^2}$ and the oxygen orbitals. We notice the shift of weight from $d_{x^2-y^2}$ to d_{3z^2} for $J_H > 1.8$, as for this large value, the other orbital becomes competitive. Panel b) shows the result for 25% hole-doped (*i.e.* $d^{8.75}$) model. The extra hole is distributed between oxygen and $d_{x^2-y^2}$ orbital for small J_H . With increasing J_H , the hole weight in d_{3z^2} keep increasing. In fact, for reasonable J_H , the d_{3z^2} can be almost a quarter of the weight of $d_{x^2-y^2}$, leading to a significant contribution to the ground state. This suggests that Hund coupling enhances multiorbital effects even for small doping.

S4. OXYGEN K -EDGE RIXS

We, here, present the O K -edge RIXS spectra using the TM_2O_7 clusters for nickelates and cuprates to explore the charge transfer excitations in these. We contrast the spectra of the nickelates with the cuprates. For evaluating the RIXS spectra, we consider the core-hole Hamiltonian given by $H_{\text{ch}} = \mathcal{H} + U_{\text{ch}} \sum_i n_i^p n_i^s$ for the oxygen K -edge [39, 49, 50]. RIXS cross-section is evaluated using the Kramers-Heisenberg formula given by,

$$\mathcal{I}_{\text{RIXS}} = \sum_f \left| \sum_{i,n,\sigma} \frac{\langle f | \mathcal{D}^\dagger | n \rangle \langle n | \mathcal{D} | g \rangle}{E_n - E_g - \hbar\omega_{\text{in}} + i\Gamma_n} \right|^2 \times \delta(E_f - E_g - \Omega). \quad (\text{S4})$$

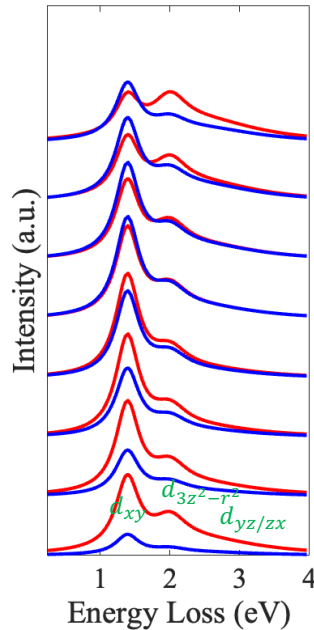


FIG. S5. Angular dependence for a set of incident energies of dd excitation evaluated using single ion (d^9) model for the σ (red) and π (blue) -polarization. This reproduces the angular dependence of dd excitations for a set of incidence energies reported in Ref [1]

Here, $|g\rangle$, $|n\rangle$ and $|f\rangle$ are the ground, intermediate, and final states with energies E_g , E_n , and E_f respectively and $\Omega (= \hbar\omega_{\text{in}} - \hbar\omega_{\text{out}})$ is the energy loss of the incoming photon. Γ is the inverse core-hole lifetime. \mathcal{D} is dipole operator given by $\mathcal{D} = \sum_{i,\alpha,\sigma} e^{i\mathbf{k}_i \cdot \mathbf{R}_i} s_{i,\sigma}^\dagger p_{i,\alpha,\sigma}$ for oxygen K -edge which involves the core $1s$ and valence $2p$ shells of the oxygen sites [39].

Fig. S4 shows the O K -edge spectra of the nickelate and cuprate. Panel a) shows O K -edge RIXS spectra for the undoped model. The brightest feature for the nickelate appears at around 5.5-8 eV, whereas in cuprates, it appears at around 3-5 eV [68] (The cuprate data are consistent with the experimental data reported for 2D cuprates [54].). The results are consistent with the picture that the cuprates are CT insulators, whereas the excitations in the nickelate appear at larger energies, which supports the mixed valence picture [39]. We also notice a weak feature at 1 eV for the nickelate and around 2 eV for the cuprates. These correspond to the dd excitations, and these energy scales are consistent with the plaquette picture discussed in appendix S2.

Panel b) shows the O K -edge RIXS spectra for the doped (50%) nickelate and cuprate. We notice an overall softening of the CT excitations in both. In the case of nickelates, a distinct feature at low energy feature at 1-2 eV appears. This feature has also been interpreted as dd excitations in Ref. [39]. For the doped cuprate model, the dd and CT excitations overlap.

S5. ANGULAR DEPENDENCE

We revisit the single site model proposed in Ref. [1] for understanding the hierarchy of the dd excitations in nickelates. The dd excitations were identified using the angular dependence of the d orbitals using a single ion picture [53]. We notice that the angular dependence for d_{3z^2} and $d_{yz/zx}$ are very close to the set of parameters reported in the paper, allowing for redundancy in the model. Here, we reanalyze the data using an alternate set of parameters; $\epsilon_{x^2-y^2} = 0$, $\epsilon_{xy} (\Gamma_{xy}) = 1.39 (= 0.2)$, $\epsilon_{3z^2} (\Gamma_{3z^2}) = 2.0 (0.3)$, $\epsilon_{yz/zx} (\Gamma_{yz/zx}) = 2.5 (1.0)$ and the approach as used in ref. [1, 53]. We can reproduce the experimentally observed data by interchanging the hierarchy of $3z^2$ and yz/zx -orbitals which is shown in Fig. S5. This suggests that the $3z^2$ need not be the farthest from $d_{x^2-y^2}$ -orbital and is indeed the lowest energy dd excitation.

S6. ANDERSON IMPURITY MODEL

The Anderson Impurity model used in our work is given by

$$\begin{aligned}
 H_{AIM} = & \sum_{\alpha} \epsilon_{\alpha} d_{\alpha}^{\dagger} d_{\alpha} + \frac{1}{2} \sum_{\alpha\beta\gamma\delta} U_{\alpha\beta\gamma\delta} d_{\alpha}^{\dagger} d_{\beta}^{\dagger} d_{\gamma} d_{\delta} \\
 & + \sum_{l\alpha} \epsilon_{l\alpha} b_{l\alpha}^{\dagger} b_{l\alpha} + \sum_{l\alpha} V_{l\alpha} d_{\alpha}^{\dagger} b_{l\alpha} + h.c.
 \end{aligned}
 \tag{S5}$$

Here, $\alpha, \beta, \gamma, \delta$ are the orbital indices of the impurity site, which represent the $3d$ -orbitals of the Ni. $l (= \{1 \cdots N\})$ is the index for the bath site. Due to computational limitations, we restrict to $N = 2$ bath sites. $\epsilon_{l\alpha}$ is the energy level of the l -th bath site with orbital α , $V_{l\alpha}$ are the hybridization strength between localized impurity electrons (d_{α}) and bath electrons ($b_{l\alpha}$). The bath levels and hybridization strengths do not exist explicitly within the DFT+DMFT functional, which integrates out these bath degrees of freedom into a Weiss field with a frequency-dependent hybridization function, $\Delta(i\omega_n)$. Here, $\epsilon_{l\alpha}$ and $V_{l\alpha}$ are obtained by fitting them to the diagonal elements of the hybridization function via the following equation:

$$\Delta_{\alpha\alpha}(i\omega_n) = \sum_{l=1}^N \frac{|V_{l\alpha}|^2}{i\omega_n - \epsilon_{l\alpha}}.
 \tag{S6}$$

The intermediate Hamiltonian with core is given by $H_n = H_{AIM} + H_{ch}$, where the core-holed effects are included in the $3d$ orbitals for the L -edge. We evaluate the Ni L -edge RIXS spectra for the AIM using EDRIXS. We use exact diagonalization to solve the AIM for both the undoped and doped materials. We restrict ourselves to two bath sites (see Sec. 2.3 in Ref. [36] for details). The calculations are performed at 300 K and use a virtual doping of the lanthanum ion to simulate the doped ($d^{8.75}$) system, and the results are shown in the Fig. 4 of the main text, which contains both the NSC and SC channels.